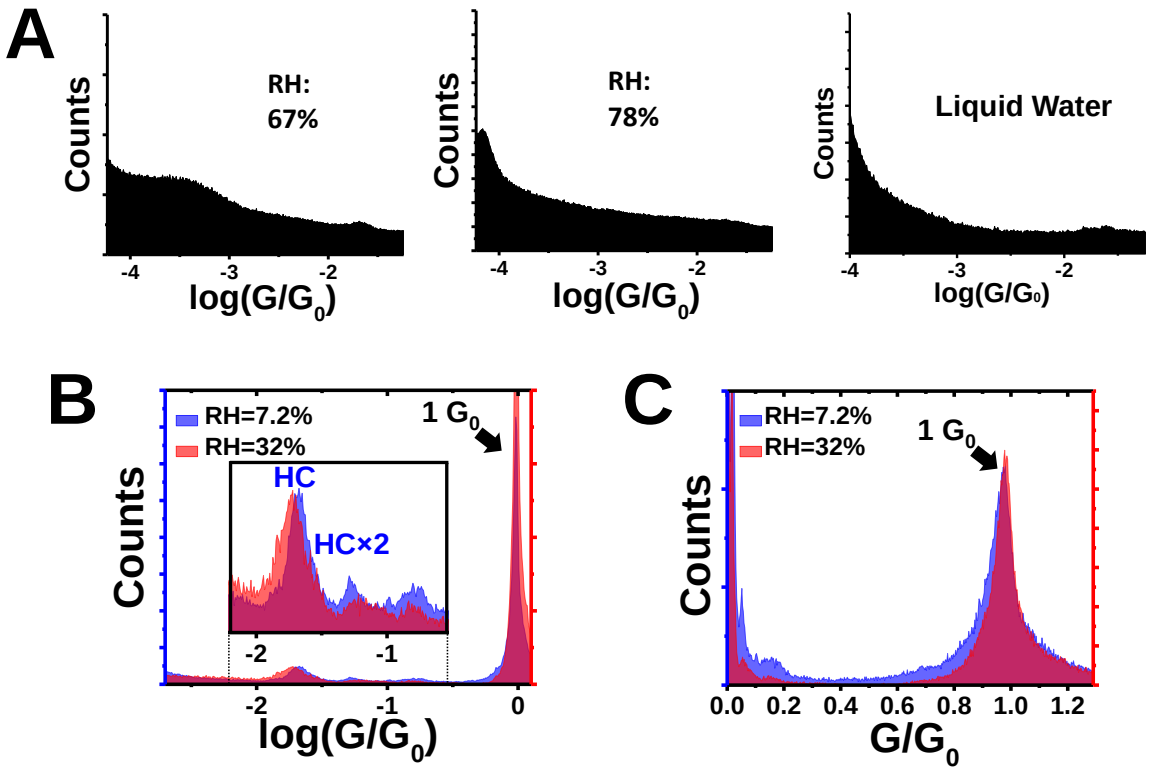


**Figure S1. Conductance histograms of water molecules at high humidity levels and liquid water, and the conductance histograms in the regime above 0.1 $G_0$. Related to Figure 2B. (A)** Conductance histograms at a relative humidity of 67%, 78%, and liquid water. No peaks show up at these high humidity levels and in liquid water. **(B)** Conductance histogram in the regime above 0.1 $G_0$ on a logarithm scale under different humidity levels, clearly showing the 1 $G_0$ peak and the HC peak. No pronounced peaks were observed near the previously reported conductance values, indicating the importance of temperature, humidity, and electrode material in the formation of water junctions. **(C)** conductance histogram in the regime above 0.1 $G_0$ on a linear scale under different humidity levels, clearly showing the 1 $G_0$ peak. Note that the HC peak at ~0.02 $G_0$ is buried in the background, limited by the resolution on the linear scale x-axis.

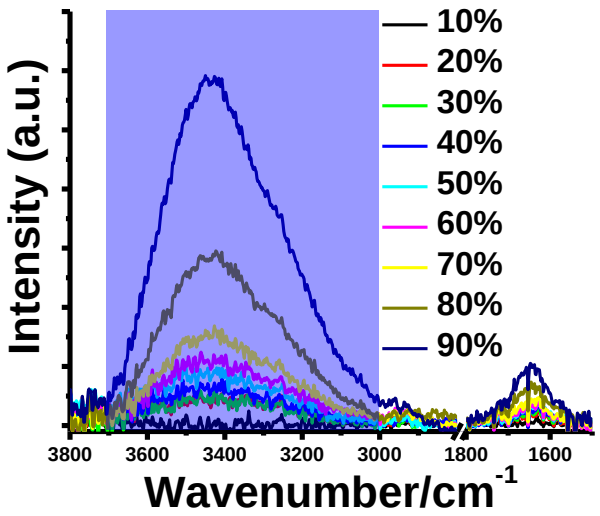


**Figure S2. IR spectra of water adsorbed on a gold surface. Related to Figure 1B.** The IR absorption (intensity) at the water stretching vibration frequency (3000-3700 $cm^{-1}$, marked as blue area) is plotted in Figure 1B. The absorption at around 1550-1800 $cm^{-1}$ is due to O-H bending. Each experiment was repeated at least three times. Based on the surface selection rule of RAIRS on metal surfaces, it is known that PM-RAIRS detects dipole components of adsorbate in the surface normal direction only; the surface parallel component cannot be detected due to the image charge screening. Thus, the extremely low PM-RAIRS intensity of water species at RH ≤ ~15% indicates that isolated water molecules are in the parallel orientation as shown in Figure 2C. Considering the conductance data and DFT calculations, this corresponds to the configuration of water molecules in regime I in the absence of strong electric field applied by the STM tip (Figure 3D); when the water molecule with a strong dipole is subject to the electric field gradient, then the isolated molecule can rearrange to the perpendicular orientation (as shown in Figure 3D) which is responsible for the LC state shown in Figure 2A and 2B. The field induced re-orientation of the isolated water molecule is schematically illustrated in Figure 3F. When a full monolayer is formed on gold at RH > ~15% (regime II), then intermolecular hydrogen bonding interactions form a network consisting of both parallel and perpendicular orientations of water molecules (as shown in Figure 2E with a hexamer model). The hydrogen bonding interactions with neighboring molecules hinder the water molecules with the parallel orientation from transition to the perpendicular orientation; thus, the HC state becomes significant in regime II. In regime III (RH > ~45% ), multiple water layers start to form on the gold surface.

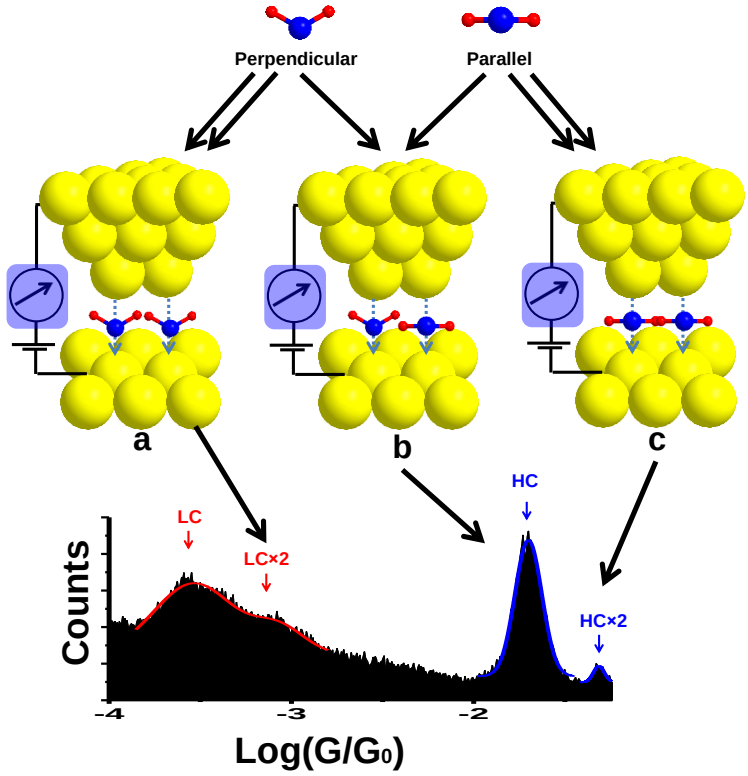


**Figure S3. Two-water molecule junctions. Related to Figure 1D.** Conductance value at the twice of the lowest peak value is a signature of single molecular junctions for the break junction techniques. Isolated water molecules with different orientations are possible in the junctions, but those corresponding to LC and HC states are the most stable configurations (according to the calculation). This gives rise to three possible configurations involving two water molecules: both molecules are in LC (a), both in HC (c), and one in LC and one in HC (b), and the corresponding values are 2×LC, 2×HC and HC (because HC has a much higher conductance). However, the peaks in the conductance histograms are broad, which could be partially due to some variations in orientations and binding geometries.

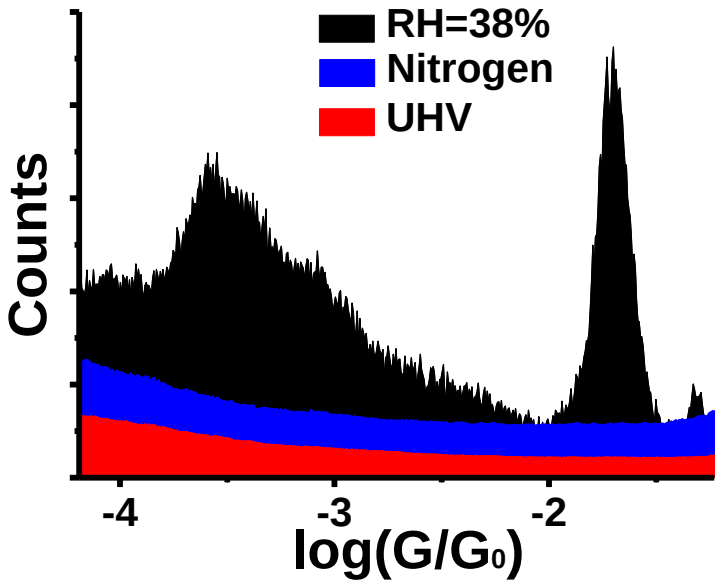


**Figure S4. Conductance histograms in vacuum, pure nitrogen gas, and under the relative humidity of 38%. Related to Figure 1D.** Conductance histograms in ultra-high vacuum (UHV, red) and nitrogen (blue) do not give any pronounced peaks. Conductance histogram at relative humidity of 38% is shown here as a comparison (black). The y-axis is shifted for better visualization. The control experiments confirmed that the peaks in conductance histogram under water vapor were due to water molecules.

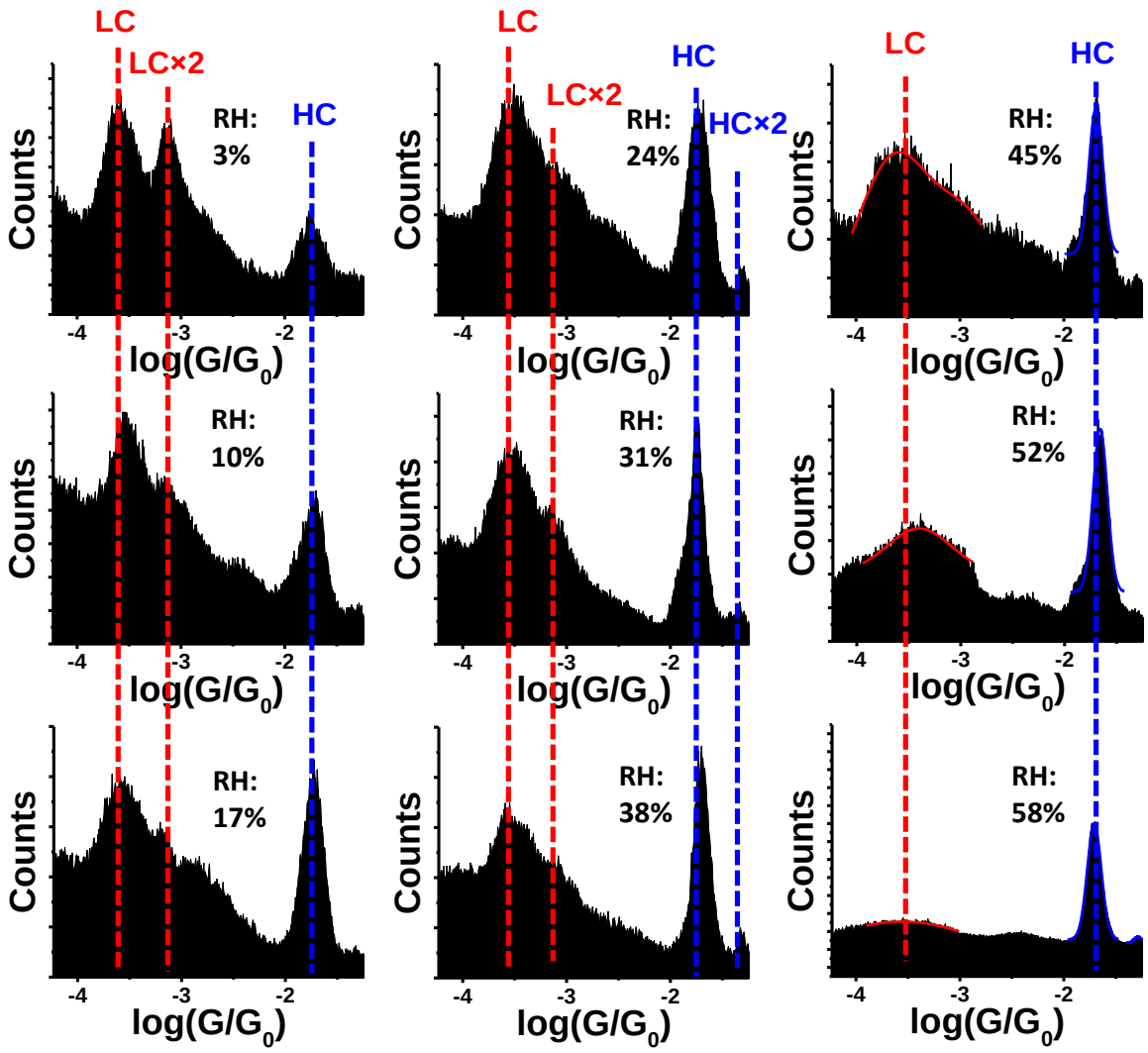


**Figure S5. Conductance histogram of water molecules at different low humidity levels. Related to Figure 2B.** Peaks for the low conductance (LC) and high conductance (HC) states are marked with red and blue dashed lines. The peak positions barely change as the humidity increases.

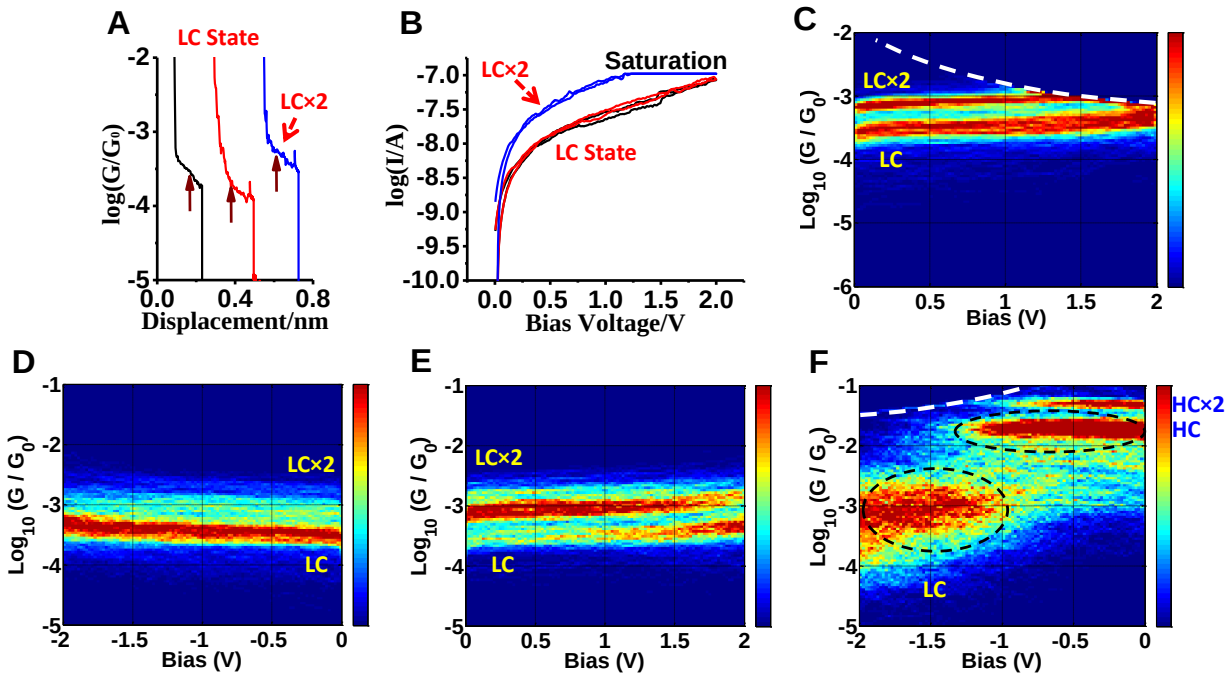


**Figure S6. Current-Voltage (I-V) measurements for both the low conductance (LC) and high conductance (HC) states with different bias polarities. Related to Figure 3A-C. (A)** Conductance vs. distance traces, each showing a plateau that corresponds to the formation of a water molecule junction in the LC state. The arrows mark the locations where the tip was fixed in position and voltage sweeping started (the blue trace starts from a LC×2 state). **(B)** Representative I-V curves of the LC and LC×2 states. Both give a nonlinear but monotonically increasing I-V signature. The current of LC×2 state reaches the saturation level of the amplifier at high bias voltages. In ~70% of the I-V curve measurement attempts, the current dropped abruptly to the noise level, which was due to the breakdown of the molecular junctions. **(C)** 2D conductance-voltage (G-V) histogram for the LC state constructed from thousands of I-V curves shows LC and LC×2 bands, where the white dashed line marks the current saturation level of the amplifier. **(D)** 2D G-V histogram of LC and LC×2 states measured with lower current amplification to avoid the saturation at high bias voltage confirms the observation in **(C)**. **(E)** 2D G-V histogram of LC and LC×2 states with the lower amplification but in the positive bias voltage direction also shows a slightly increasing G-V characteristic. Panel **(C)**, **(D)** and **(E)** confirm that the LC state is stable without switching upon increasing the bias to 2V. **(F)** 2D G-V histogram of HC and HC×2 states in the negative bias voltage direction shows the switching from the HC to the LC state, consistent with Figure 3C, where the white dashed line marks the current saturation level of the amplifier. These results show that a high bias voltage induces conductance switching from the HC state to the LC state only, and the switching does not depend on the bias voltage polarity.

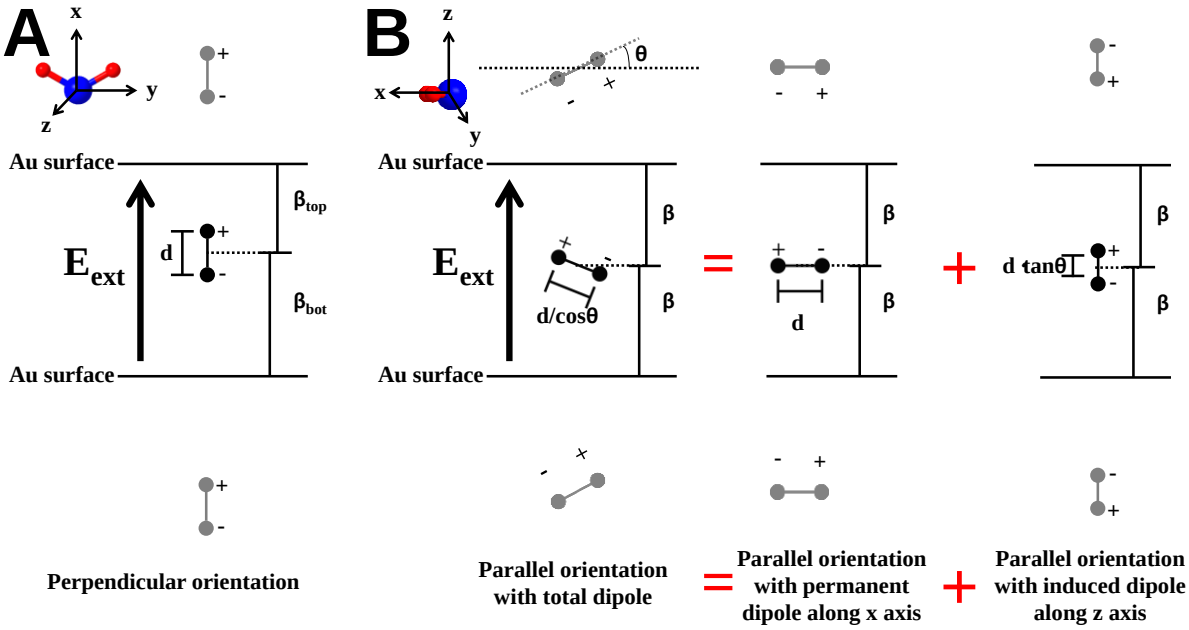


**Figure S7. Schematic diagrams showing a water molecule (represented with a dipole) in different orientations under an electric field. Related to Figure 3D.** Notice that the x-axis is always defined as the direction along the water dipole and the z-axis is defined as the perpendicular direction to the water molecular plane. **(A)** The perpendicular orientation under a large electric field. **(B)** The parallel orientation under a large electric field. The total dipole can be divided into two orthogonal components, where the direction along the x-axis is water's permanent dipole (includes the effects from the image fields) and the direction along the z-axis is the dipole induced by the external electric field (includes the effects from the image fields).

**Table S1**. **Electronic coupling strengths (Γ) for different orientations with different σ values. Related to Figure 2C.** This shows the robustness of the electronic coupling strengths rankings for different orientations (Parallel > Perpendicular-L > Perpendicular-R > Sideway-L). σ is defined as the width of the distribution in Eq. 2.

| $\sigma$ (eV) | Sideway-L $\Gamma$ (eV) | Perpendicular-R $\Gamma$ (eV) | Perpendicular-L $\Gamma$ (eV) | Parallel $\Gamma$ (eV) |
|---|---|---|---|---|
| 0.750 | 0.340 | 1.670 | 2.416 | 2.680 |
| 0.500 | 0.323 | 1.497 | 2.312 | 2.876 |
| 0.125 | 0.468 | 1.555 | 2.371 | 2.981 |
| 0.050 | 0.544 | 1.414 | 2.264 | 3.017 |
| 0.025 | 0.433 | 1.670 | 1.860 | 2.961 |

**Table S2. Computed conductance ratios between the parallel orientation and the perpendicular orientation at selected energy gaps ΔE between the water HOMO orbital and the Au Fermi level. Related to Figure 2C.**

| ΔE (eV) | $G_{parallel}$ / $G_{perpendicular}$ |
|---|---|
| –3.66 | 3.1 |
| –2.86 | 5.9 |
| –2.04 | 10.4 |
| –1.22 | 18.7 |

**Supplemental Experimental Procedures**

**Calculations of energy for parallel and perpendicular orientations under external electric fields**

We calculated the energies of a water molecule in the parallel and perpendicular orientations under an external electric field by considering the polarizability of water and the image dipoles caused by the two metal electrodes. For water in a perpendicular orientation (Figure S7A), the total energy gained ($U_{ver}$) from the electric field-dipole interaction is given by[1],

$$U_{ver} = -\mathbf{E}_{\mathbf{ext}} \cdot \boldsymbol{\mu}_{\mathbf{ver}} - \frac{1}{2}\mathbf{E}_{\mathbf{img\text{-}t}} \cdot \boldsymbol{\mu}_{\mathbf{ver}} - \frac{1}{2}\mathbf{E}_{\mathbf{img\text{-}b}} \cdot \boldsymbol{\mu}_{\mathbf{ver}} + \frac{1}{2}\left(\mathbf{E}_{\mathbf{ext}} + \mathbf{E}_{\mathbf{img\text{-}t}} + \mathbf{E}_{\mathbf{img\text{-}b}}\right) \cdot \left(\boldsymbol{\mu}_{\mathbf{ver}} - \boldsymbol{\mu}_{\mathbf{0}}\right), \quad \text{Eq. S1}$$

The first three terms in Eq. S1 are the interactions between the electric field and the dipole. The last term includes the energy cost to polarize water. $E_{ext}$ is the external electric field. $\mu_{ver}$ is the total dipole of the water molecule after being polarized. $\mu_0$=1.85 D is the permanent dipole of water, $E_{img\text{-}t}$ and $E_{img\text{-}b}$ are the image field by the top and bottom electrodes. $\mu_{ver}$, $E_{img\text{-}t}$ and $E_{img\text{-}b}$ can be expressed as[1],

$$\boldsymbol{\mu}_{\mathbf{ver}} = \boldsymbol{\mu}_{\mathbf{0}} + 4\pi\varepsilon_0\alpha_x\left(\mathbf{E}_{\mathbf{ext}} + \mathbf{E}_{\mathbf{img\text{-}t}} + \mathbf{E}_{\mathbf{img\text{-}b}}\right), \quad \text{Eq. S2}$$

$$\mathbf{E}_{\mathbf{img\text{-}t}} = -\frac{\boldsymbol{\mu}_{\mathbf{ver}}}{4\pi\varepsilon_0 d^2}\left(-\frac{1}{2\beta_{top}+d} - \frac{1}{2\beta_{top}-d} + \frac{1}{\beta_{top}}\right), \quad \text{Eq. S3}$$

$$\mathbf{E}_{\mathbf{img\text{-}b}} = -\frac{\boldsymbol{\mu}_{\mathbf{ver}}}{4\pi\varepsilon_0 d^2}\left(-\frac{1}{2\beta_{bot}+d} - \frac{1}{2\beta_{bot}-d} + \frac{1}{\beta_{bot}}\right), \quad \text{Eq. S4}$$

$\varepsilon_0$ is the vacuum permittivity. $\alpha_x$ = 1.48 Å$^3$ is the polarizability along the dipole direction of water[2,3](Figure S7A). $d$ = 0.63 Å is the length of the dipole. $\beta_{top}$ = 3.2 Å and $\beta_{bot}$ = 2.9 Å are the distance from the dipole to the top electrode and bottom electrode respectively (Figure S7A). $\beta_{top}$ and $\beta_{bot}$ are obtained from our DFT calculations.

For water in the parallel orientation, because of the polarizability along the *z*-axis, the total dipole $\mu_{par}$ can be divided into two orthogonal directions (Figure S7B). The total energy gained $U_{par}$ is the sum of these two components along the two orthogonal directions.

$$U_{par} = U_{par\text{-}x} + U_{par\text{-}z}, \quad \text{Eq. S5}$$

where $U_{par\text{-}z}$ can be calculated using the same way as that for the perpendicular orientation by combing Eqs. S1-4, while $U_{par\text{-}x}$ can be expressed as[1],

$$U_{par\text{-}x} = -\mathbf{E}_{\mathbf{img\text{-}x}} \cdot \boldsymbol{\mu}_0, \quad \text{Eq. S6}$$

$E_{img\text{-}x}$ is the image field along x-axis caused by the top and bottom electrode (Figure S7B) and can be expressed as[4],

$$\mathbf{E}_{\text{img-x}} = -\frac{\boldsymbol{\mu}_{\text{par}} \cdot \cos\theta}{4\pi\varepsilon_0 d^2}\left[-\frac{1}{\beta - \frac{d}{2}} + \frac{2}{\sqrt{d^2 + 4\left(\beta - \frac{d}{2}\right)^2}}\right], \quad \text{Eq. S7}$$

$\theta$ is the angle between the $\mu_{par}$ and the water molecular plane (Figure S7B). $\beta$ = 2.9 Å is the distance between the dipole and the electrode for parallel orientation, which is obtained from DFT calculations. Notice that the two image dipoles have the same electric field for parallel orientation. The two orthogonal directions of the $\mu_{par}$ can be expressed by the following equations (Figure S7B),

$$\begin{aligned}\boldsymbol{\mu}_{\text{par}} \cdot \cos\theta &= \boldsymbol{\mu}_{\mathbf{0}} + 8\pi\varepsilon_0\alpha_x\mathbf{E}_{\text{img-x}} \\ \boldsymbol{\mu}_{\text{par}} \cdot \sin\theta &= 8\pi\varepsilon_0\alpha_z\mathbf{E}_{\text{img-z}} + 4\pi\varepsilon_0\alpha_z\mathbf{E}_{\text{ext}}\end{aligned}, \quad \text{Eq. S8}$$

$E_{img\text{-}z}$ is the image field along z-axis and can be calculated by Eq. S3. $\alpha_z$ = 1.7 Å$^3$ is the polarizability along the *z*-axis[2,3].

The initial energy (at zero electric field) for parallel orientation is calculated by 2×parallel energy in Figure 2D and the initial energy for perpendicular orientation is calculated by the sum of perpendicular-L energy and perpendicular-R energy in Figure 2D. The sum of the initial energy and the energy gained from the electric field as calculated above is plotted in Figure 3D.

**Populations of LC/HC states versus the bias voltage in Figure 3E**

Under equilibrium, the populations of HC and LC state are given by,

$$\begin{aligned}&[\mathrm{HC}] \longleftrightarrow [\mathrm{LC}] \\ &\Delta U = -\mathrm{k}_B\mathrm{T}\ln\frac{[\mathrm{LC}]}{[\mathrm{HC}]}\end{aligned}, \quad \text{Eq. S9}$$

where $\Delta U$ is the energy difference of the two states, $k_B$ is the Boltzmann constant and T is temperature in K. From Eq. S9, we express the population of the HC state as

$$\begin{aligned}P(\mathrm{HC}) &= \frac{1}{1 + e^{-\frac{\Delta U}{k_B T}}} \\ \Delta U &= U_0 + \frac{V_{bias}}{d_{gap}} \cdot \mu\end{aligned}, \quad \text{Eq. S10}$$

where $U_0$ is the energy difference in the absence of electric field. $V_{bias}$ is the bias voltage and $d_{gap}$ is the distance between the two electrodes. $\mu$ is water molecular dipole. We calculated the population of HC state from the counts within the full-width-half-maximum range of the HC conductance peak as shown in

Figure 3C. The population of HC state versus bias voltage was fitted with Eq. S10 and shown in Figure 3E.

**Relation between single molecular conductance and electron transfer rate in donor-bridge-acceptor (DBA) system**

The electron transfer rate in DBA system $k_{DA}$ can be related to the molecular conductance $g$ in the following way[42],

$$g \approx \frac{8e^2}{\pi^2 \Gamma_D^L \Gamma_A^R F} k_{DA}$$

$$F = \frac{e^{-(\lambda + E_{AD})^2 / 4\lambda k_B T}}{\sqrt{4\pi\lambda k_B T}}$$ , Eq. S11

$e$ is the charge of electron. $\Gamma_D^L$ and $\Gamma_A^R$ are the coupling strengths between donor and left electrode, between acceptor and right electrode respectively, which are assumed to be 0.5 eV. $F$ is the Franck-Condon factor. $E_{AD}$ is the electronic energy gap between the donor and acceptor, which is assumed to be 0 eV. $\lambda$ is the reorganization energy, taken to be 0.5 eV. Eq. S11 allows conversion of single molecule conductance to electron transfer rate. The converted electron transfer rates are plotted in Figure 4B. These values are based on the "static" high conductance and low conductance values.

**Conductance calculations**

We carried out the conductance computations for the parallel and perpendicular orientations using the DFT derived Au-water interaction values. In the calculations, the electrodes were simulated using the same cluster model used in deriving the Au-water coupling (see computational methods). The continuum of lead states is represented by a set of 2832 energy levels, each coupled to the molecule and each with a damping term **γ** (=0.02 eV) that causes the density matrix for the leads to approach an equilibrated thermal distribution. The Hamiltonian of the water and two Au electrodes is represented by the Kohn-Sham matrix obtained in the water-Au coupling calculations. Details of the conductance formulism was presented in our previous calculations[5]. At a bias voltage of 0.05 V, the computed conductance ratio between the parallel and perpendicular-L orientations ranges from 3 to 19, depending on the relative energy between the water HOMO orbital and the Au Fermi level. While the calculations correctly captured the observed conductance trends, the disparity between theory and experiments may be caused by the accuracy of the DFT methodology (the DFT functional and basis sets), the size of the Au cluster model, and thermally induced structural fluctuation contributions to the conductance. Structural fluctuations will reduce the water-Au interactions more significantly for weakly absorbed conformers than those of the strongly absorbed ones.

**Supplemental References**


1 Maschhoff, B. L. & Cowin, J. P. (1994). Corrected electrostatic model for dipoles adsorbed on a metal surface. *J. Chem. Phys.* **101**, 8138-8151.

2 Wan, Q., Spanu, L., Galli, G. A. & Gygi, F. (2013). Raman Spectra of Liquid Water from Ab Initio Molecular Dynamics: Vibrational Signatures of Charge Fluctuations in the Hydrogen Bond Network. *J. Chem. Theory Comput.* **9**, 4124-4130.

3 Ge, X. & Lu, D. (2017). Molecular polarizability of water from local dielectric response theory. *Phys. Rev. B* **96**, 075114.
4 Carrasco, J., Michaelides, A. & Scheffler, M. (2009). Insight from first principles into the nature of the bonding between water molecules and 4d metal surfaces. *J. Chem. Phys.* **130**, 184707.
5 Liu, C. *et al.* (2016). Engineering nanometre-scale coherence in soft matter. *Nat. Chem.* **8**, 941-945.